Universidad de Alcalá
BIBLIOTECA

Document downloaded from the institutional repository of the University of Alcala: http://ebuah.uah.es/dspace/

This is a posprint version of the following published document:

Martínez Muñoz, M., Díez Jiménez, E., Sánchez Montero, R., López Espí, P.L. & Martínez Rojas, J.A. 2019, "Analysis of the geometric parameters influence in PCB fixtures for 2D multipole magnetization patterning of thin layer micro-magnets", International Journal of Applied Electromagnetics and Mechanics, vol. 61, no. 1, pp. 59-71.

Available at https://dx.doi.org/10.3233/JAE-180121

© 2019 The authors

(Article begins on next page)

This work is licensed under a

Creative Commons Attribution-NonCommercial-NoDerivatives 4.0 International License.

Analysis of the geometric parameters influence in PCB fixtures for 2D multipole magnetization patterning of thin layer micro-magnets

Miriam Martinez-Muñoz [a], Efren Diez-Jimenez [a], Rocio Sanchez-Montero [a], Pablo Luis Lopez-Espi [a] and Juan Antonio Martinez-Rojas [a]

[a] *Dpto. Teoría de la Señal y Comunicaciones, Universidad de Alcalá, Ctra. Madrid-Barcelona, Km 33,66, Alcalá de Henares, 28871, Spain. Email: efren.diez@uah.es*

Abstract. Magnetic actuators, magnetic gears, vibrational energy harvesters and other micro-electromagnetic devices requires micro-magnetic rotors with alternant magnetizations to optimize their performance. Different approaches have been used for multipole magnetization of micro-magnets like fixed micro-fixtures, thermomagnetic patterning or laser machining. The main limitation of previous techniques is that the inversion of the magnetic polarizations is done only partially. In this work, a concept based on 2D multipole magnetization printing of micro-magnets is proposed and analyzed to overcome current limitations. The fixtures are designed to be printed on a standard 35 µm PCB. The dependence of the magnetizing field with respect to the geometrical parameter of the fixture is analyzed. Maps of the required current for the magnetizing fields are also given. Some design recommendations to optimize the magnetizing field and to minimize current, thus the heat, are given.

Keywords. Magnetizing fixtures, magnetic polarization patterning, micro-magnets

1. Introduction

One of the most important factors in the development of microelectronics is the miniaturization of mechanical systems. Magnetic actuators, motors [1]–[4], clutches [5], micro-magnetic gears [6], vibrational energy harvesters [7] and other micro-electromagnetic devices [8] have aroused great interest for the microscale in recent years. In consequence, the size of the magnetic rotors and components need to be reduced.

At present, micro-magnets are machined out of larger bulks and then the individual micro-magnets are axially magnetized and finally assembled into the microsystem. This is a costly manufacturing process and since most magnets are magnetized prior to assembly, handling and positioning these micro-magnets is not straightforward. Magnetizations are also possible after assembly [9]–[11]. As a solution to the above technical problems, multipole magnetization of assembled micro-magnets can be performed.

Commonly, multipole magnetic structures can be created by pulse magnetization [12], [13]. When using a magnetizing device made from copper wire and a high pulse

current passing through, it produces a magnetizing field strong enough to produce a permanent magnetization in the micro-magnet [14]. Although pulsed magnetization is a standard process in the macro scale, it is not the same for micromagnets, since the process is more complicated due to the smaller size of the fixtures in relation to the micromagnets [15].

Different techniques have been tested to achieve multipolar magnetization of micromagnets. The main objective of these techniques is to achieve large field peak variations with fine periodic spacing, also correlated with high spatial field gradients. Previous developments have demonstrated that combining fixed electrical conductors and soft magnetizing heads to print the submillimeter period of the north/south magnetic poles results in the creation of multipole on hard magnetic films [15].

Furthermore, patterns with lateral dimensions with lower values than ~70 μm have been produced by thermomagnetic patterning, although only on the surface of the layer (1-μm depth). In addition, to selectively reverse the magnetizing direction of a hard magnetic layer, a technique based on the use of a single soft magnetic head laser machined was developed [16]. The above techniques present the limitation that the magnetic product remaining in the polarized volumes is less than the potential that can be reached. The inversion of the magnetic polarization is done only in a superficial way.

A technique with a totally different approach has been proposed for the case of the magnetization pattern in macro-scale magnets [18]. In this way, magnetization patterns are generated by magnetizing locally the magnet bulk with alternative polarization. By moving X – Y the magnetizing fixture to different locations above the magnet, the volumes can be magnetized as desired. This is how pixel magnetization patterns can be created. A successful result has been obtained for macro-scale magnets obtaining a magnetic pixel size of 4 mm [19] and for thicknesses greater than 3 mm.

In the present work, a concept based on printing 2D multipolar magnetization at the micro-magnet scale is analyzed. The correct design and optimization of these small fixtures are necessary so that the current is lower and consequently so will be the heat generated that can damage the fixture. The first step is the trade-off analysis trying to minimize the necessary current for a certain level of the magnetizing field while maintaining a good pixel size.

First, in this work, a trade-off analysis applied to 100 μm thick micromagnets has been performed. Fixtures are designed to be manufactured in a conventional 35 μm Printed Circuit Board (PCB). The dependence of the magnetizing field in relation to the geometric factors of the fixture is determined. These maps make possible to preselect a suitable energy source as well as to determine the increase of the temperature. Some design guidelines are given to optimize the magnetization field and minimize current and therefore heat.

This paper is organized as follows: section 2 presents a design of the fixture, section 3 describes the finite element model. The 4. Simulation Descriptions and Post-processing are described in section 4, results are presented in section 5, and an example of application of the results is described in section 6. Finally, the main conclusions are presented in section 7.

2. Definition of the fixture for 2D magnetic patterning

As mentioned above, the 2D magnetic patterning consists of a pair of movable magnetic coils that magnetize locally the permanent magnet bulk, creating the sough pattern. They

are above and below the permanent magnet bulk. This makes it possible to magnetize complex bulks such as hollow cylinders or plates with alternative polarization, figure 1.

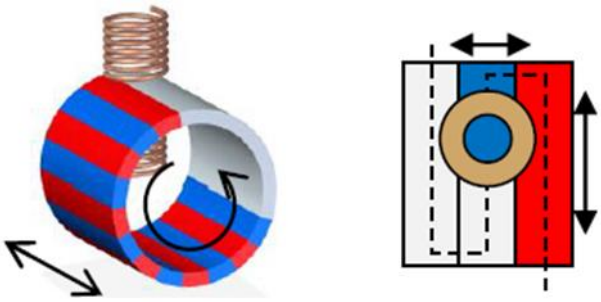

Figure 1. Motion paths for magnetizing a hollow cylinder or a plate with alternative polarizations.

The denomination of the different parameters is shown in the geometrical diagram of Figure 2. The fixture, which is an asymmetrical device, is composed of: sample to be magnetized (1), top and a bottom cylindrical coils (2) and the inner core (3). Both coils are connected in series so that a magnetizing field is generated in the same direction. Five geometrical parameters have been defined: e – thickness of the permanent magnet bulk, R_{INT} – inner radius of the coil, R_{EXT} – outer radius of the coil. H_C – height of the coil, H_{CORE} – height of inner core.

A current circulates through each coil. This current is considered uniformly distributed across the cross-section and perpendicular to the cross-section. To simplify the simulation, the space between coils will be considered as air or vacuum.

In the design, the coil height value has been taken as the typical thickness of copper PCB tracks, with a value of 35 µm (1 oz).

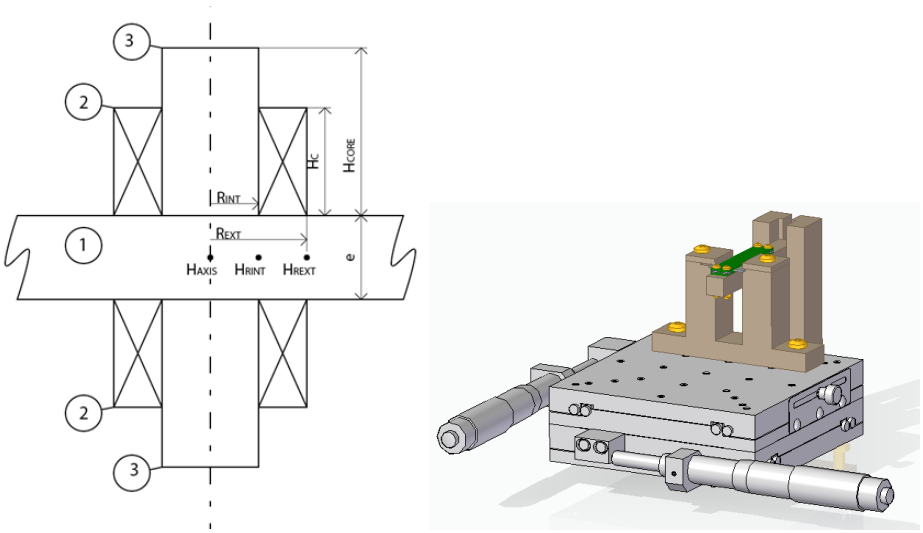

Figure 2. Left - Diagram and parameters of the axisymmetric fixture model. Right – Conceptual model of the magnetizing system: moving table, rigid structure for magnet holding and PCB (green plates).

An empty inner core has been considered. Even if a ferromagnetic material core could raise the total magnetizing field, other issues may appear. The main drawback is the magnetic interaction that acts between a ferromagnetic core and those adjacent magnet volumes. The forces between fixture and magnet sample will be also a pitfall when moving the fixture along the magnet. Moreover, the inductance of the coils would be much larger. In a first approach, the inductance of a solenoid coil can be expressed as $L = \frac{\mu N^2 A}{l}$, where l is the length of the coil, A is the cross-section area, N is the number of turns and μ is the permeability of the core. Inductance affects directly to the time constant of the RL electric circuit, which is $\tau = \frac{L}{R}$. Thus, the speed of the 2D patterning is directly related to the magnetic permeability of the core. Ferromagnetic material cores have permeabilities ranging from 1000 to 10000, therefore speed of patterning would be orders of magnitude slower.

Figure 3 shows an example of the axisymmetric simulation model. Figure 3-a represents the top an bottom coil, an empty core and the magnetizing sample is between the coils. As shown in figure 3-a, the magnetizing field intensity generated by the fixtures has two symmetries: axial and middle section plane. The lowest values are achieved in the middle section of the sample space. Figure 3-b shows the magnetic field intensity along a radius of the middle section. This magnetic field has a maximum in the axis and then it decreases as long as it approaches to the end of the coil. Just around the end of the coil, the magnetic field intensity vector is inverted to negative values. These negative values have typically an order the magnitude lower than the maximum so the effect on the adjacent magnetizations is small. The variation in respect to the radius depends on the geometry so it is necessary to characterize the shape of the applied magnetizing field for each geometrical parameter combination.

For simplicity, the magnetic field intensity (H) will be only calculated at three key points: point H_{AXIS}, located at the middle section of the sample in the symmetry axis; point $H_{RINT,}$ located at the middle section of the sample and radially at the start of the coil and H_{REXT}, located at the middle section of the sample and radially at the end of the coil. The magnetizing field at first point H_{AXIS} will represent the minimum magnetizing field that will be available in the axis. In a simplified manner, it is considered that if this H_{AXIS} is larger than the magnetic coercivity of the material, the sample would be 100% magnetized along the axis.

Other analysis can be done from the magnetic field at those three key points. For example, the magnetic field at second point H_{RINT} divided by the magnetic field at H_{AXIS} indicates the amount of magnetizing field at the beginning of the coil, representing the width of the magnetized pixel. Another example, magnetic field at third point H_{REXT} in respect to the magnetic field at H_{AXIS} and/or in respect to the magnetic field at H_{RINT}, indicates the type of transition between magnetized pixels. The sharpness or the smoothness between adjacent pixels with alternative polarization can be described by those parameters.

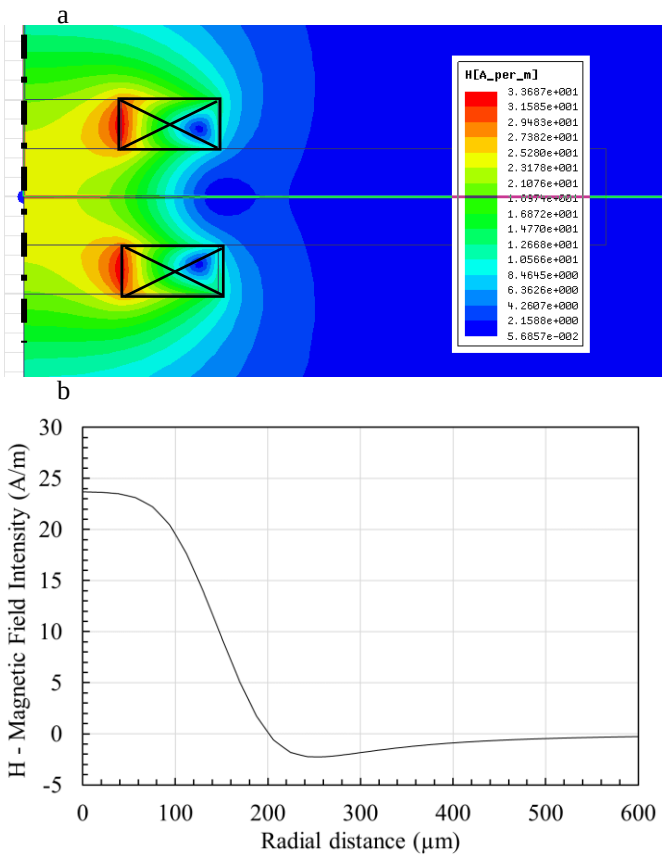

Figure 3. a) H - magnetic field intensity distribution (e = 100 µm, HC = 50 µm, RINT = 100 µm, REXT = 200 µm); b) H - magnetic field intensity along a middle section radius.

3. Finite Element Model

All the calculations have been done using a finite element model (FEM) software for electromagnetic fields. The solver chosen is the magnetostatic solver from ANSYS Maxwell. The magnetostatic field solution verifies the following two Maxwell's equations:

$$\nabla \times \vec{H} = \vec{J} \text{ and } \nabla \cdot \vec{B} = 0$$

With the following relationship applicable to each material:

$$\vec{B} = \mu_0(\vec{H} + \vec{M}) = \mu_0 \cdot \mu_r \cdot \vec{H} + \mu_0 \cdot \vec{M}_p \qquad (1)$$

Where H is the magnetic field intensity, B is the magnetic field density, J is the conduction current density, M_p is the permanent magnetization, μ_0 is the permeability of vacuum and µr is the relative permeability.

For nonlinear materials, the dependency between the H and B fields is nonlinear and can be isotropic or orthotropic (in the case of anisotropic behavior, is a tensor). If

nonlinearity occurs in soft materials (with negligible hysteresis) simultaneously with orthotropic behavior, the software requires that BH curves for the principal directions in the respective material(s) are provided. From these curves, the energy dependency on H is extracted for each of the respective principal directions and it is used in the process of obtaining the nonlinear permeability tensor used in the Newton-Raphson iterative solution process.

There are major advantages of this formulation over other existing ones, including using considerably fewer computational resources (due to the scalar nature of the DOFs), not requiring a gauge due to excellent numerical stability, significantly reducing cancellation errors, and capable of automatically multiplying connected iron regions [17].

The magnetostatic solver calculates the magnetic field distribution produced by a combination of known DC current density vector distribution and a spatial distribution of objects with permanents magnetization. It is also possible to apply boundary conditions to a model such that the simulation of the immersion of a device into an external magnetic field is also possible. In this latter case, the boundary conditions are applied in such a way that Maxwell's equations are not violated inside the domain of the solution or at the boundaries.

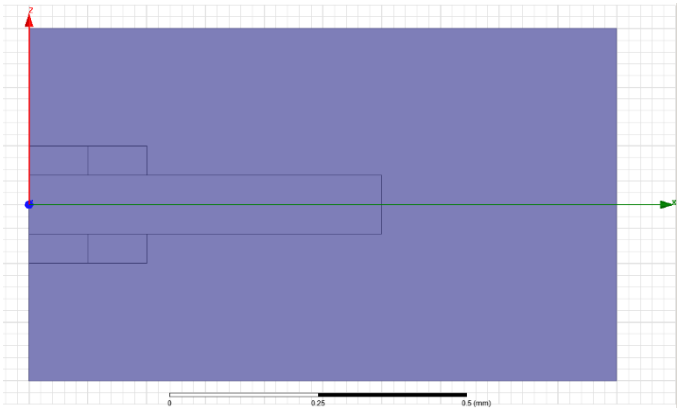

Figure 4. 2D axisymmetric parametric FEM model distribution (e = 100 µm, R_{INT} = 100 µm, R_{EXT} = 200 µm, H_C = 35 µm).

The geometrical model for the FEM is shown in figure 4. It is an axisymmetric 2D model. Z-axis is the axial symmetry axis. In this model, all the geometrical parameters from figure 2 can be modified in any combination by the software. The mesh size of the model is proportional to the main geometrical parameters e and R_{INT}, being finer in the surroundings interfaces. An example of the mesh is shown in figure 5.

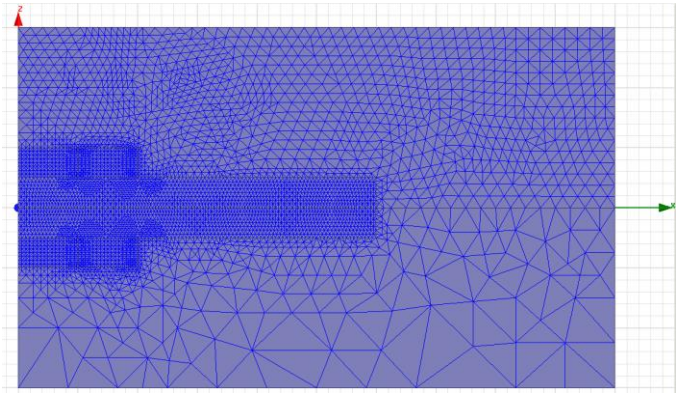

Figure 5. Detail of the initial (e = 100 μm, R_{INT} = 100 μm, R_{EXT} = 200 μm, H_C = 35 μm).

The materials considered in the simulation are two: vacuum and copper. The values chosen for the properties are: magnetic permeability of vacuum $\mu_0 = 4\pi \cdot 10^{-7}$ H/m, relative permeability of copper $\mu_{rCu} = 0.99991$ and conductivity of copper at 20ºC $\sigma_{Cu} = 5.8 \cdot 10^7$ S/m.

As boundary conditions, a "Balloon" type condition has been applied in the external edges. Balloon condition models the region outside the drawing space as being near "infinitely" large — effectively isolating the model from other sources of current or magnetic fields. Moreover, axisymmetric condition around Z axis has been imposed.

The external excitation of the model is a current per area uniformly distributed in the copper coil cross section, pointing perpendicular outside of the XZ plane. The default value for this current is i=1 A/mm^2, allowing a normalization of the results since magnetizing field depends directly on current.

Some of the results are presented in respect to this current value, chosen as a value for normalization since the generated magnetizing field is directly proportional in magnitude to the current.

4. Simulation Descriptions and Post-processing

Each simulation corresponds to a single combination of the four geometrical parameters described in figure 2. Each simulation has been done considering a stationary condition.

The solver uses an adaptive meshing solver. Typically, three to four iterations on the mesh have been sufficient for a correct convergence of the simulation. The total number of triangular elements has been around 20000 elements. The mesh has been designed for achieving less than 0.03% of energy error within a simulation time of fewer than 5 seconds per simulation.

The simulations have been done in a workstation with an Intel Core i4-4690 with 8Gb of RAM memory. A thickness of e = 100 μm has been analyzed in combination with the rest of the parameters. The combinations are listed in table 1.

Nº sim.	e (μm)	H_C (μM)	R_{INT} (μM)	R_{EXT} (μM)
1	100	35	12.5 TO 200 (12.5 STEP)	R_{INT} + (12.5 TO 200)

Table 1. Simulation plan description.

The simulation plan has been proposed in order to assess how the width of the coil affect to the magnetizing field and to determine the point where increasing in coil height is not efficient. Each simulation returns the magnetic field intensity in the points described in section 2, H_{AXIS}, H_{REXT} and H_{RINT}. Besides that, in a post-processing phase, other useful calculations have been calculated from these three values. Expressions for those calculations are:

$$\%\, Pixel = \frac{H_{RINT}}{H_{AXIS}} \cdot 100 \qquad (2)$$

$$k = \frac{H_{RINT} - H_{REXT}}{R_{INT} - R_{EXT}} \qquad (3)$$

$$\%\, Out = \frac{H_{REXT}}{H_{AXIS}} \cdot 100 \qquad (4)$$

Expression (2) provides a measurement of the decay of the magnetizing field at the beginning of the coil. Expression (3) represents the slope in the variation of the magnetizing field from the beginning of the coil to the end. Expression (4) provides a measurement of the decay of the magnetizing field at the end of the coil, showing the effects that a determined local magnetization may have on the adjacent volumes.

The value for the resistivity of the copper is critical for the right determination of the voltage. However, the selection is not trivial since the cylinder will heat up by joule effect, thus resistivity property varies. Indeed, the maximum current admissible, thus the maximum magnetizing field, by the cylinder will depend on the rise of the temperature. As a first approximation, the value chosen is the corresponding to the resistivity operating at an intermediate temperature between 20º and the fusion temperature of the copper which is 1085 °C. Therefore,

$$\rho = \rho_{20} \cdot (1 + \alpha \cdot \Delta T) = 1.71 \cdot 10^{-8}(1 + 3.9 \cdot 10^{-3} \cdot (545 - 20)) = 5.13 \cdot 10^{-8}\ \Omega m.$$

In this calculation, skin effect has been considered negligible. This assumption is fairly valid provided that pulse duration is longer than 10 ms for copper conductors [18].

In terms of thermal behavior, the power density generated by the coil can be expressed as:

$$P_{Vol} = \frac{I^2 \cdot R}{H_C \cdot \pi \cdot (R_{EXT}{}^2 - R_{INT}{}^2)} = \frac{(j \cdot S)^2 \cdot \rho \cdot \frac{l}{S}}{H_C \cdot \pi \cdot (R_{EXT}{}^2 - R_{INT}{}^2)} = \frac{j^2 \cdot S \cdot \rho \cdot l}{H_C \cdot \pi \cdot (R_{EXT}{}^2 - R_{INT}{}^2)} = \frac{j^2 \cdot \rho \cdot H_C \cdot (R_{EXT} - R_{INT}) \cdot 2\pi \cdot (R_{INT} + \frac{R_{EXT} - R_{INT}}{2})}{H_C \cdot \pi \cdot (R_{EXT}{}^2 - R_{INT}{}^2)} = j^2 \cdot \rho \qquad (6)$$

This implies that power density, and thus temperature raise per volume, is independent of the geometry of the coil. However, the current needs to be adequately large for achieving the required magnetizing field.

5. Results & Discussion

In this section, results and discussion for the simulation results are presented.

Figures 6-9 present the results from simulation number 1. In this simulation, the magnetizing field has been analyzed by combining R_{INT} and R_{EXT} for a single height of the coil value H_C = 35 µm.

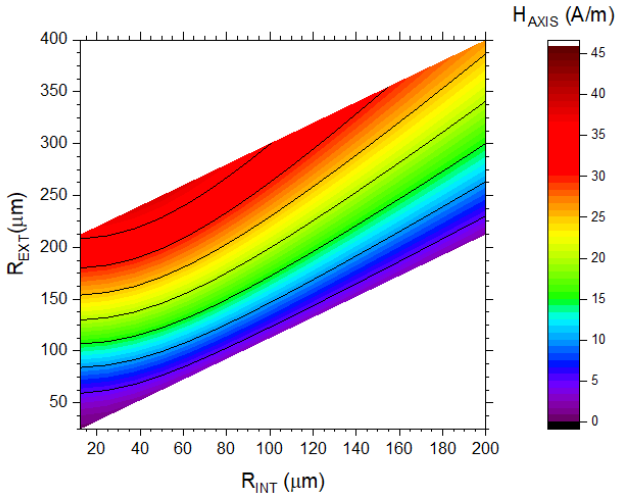

Figure. 6. HAXIS in respect to RINT and REXT for e = 100 µm and Hc = 35 µm.

Figure 6 presents a contour map of the magnetizing field H_{AXIS} for different combinations of R_{INT} and R_{EXT}, with a thickness e and a coil height H_C fixed. The values vary from 0.5 to 38 A/m for a current of 1 A/mm^2. The maximum values are achieved at R_{INT} = 50 µm and R_{EXT} = 250 µm. The minimum values are achieved at R_{INT} = 125 µm and R_{EXT} = 25 µm. For any R_{INT} value, magnetizing field increases when increasing R_{EXT}, i.e. the thicker is the coil, the larger the magnetizing field. The behavior of H_{AXIS} is almost linear with respect to R_{INT} and R_{EXT}. This means that it can be worth in terms of the magnetizing field to use thick coils. However, by using thicker coils the pixel will also be larger, decreasing the pattern resolution.

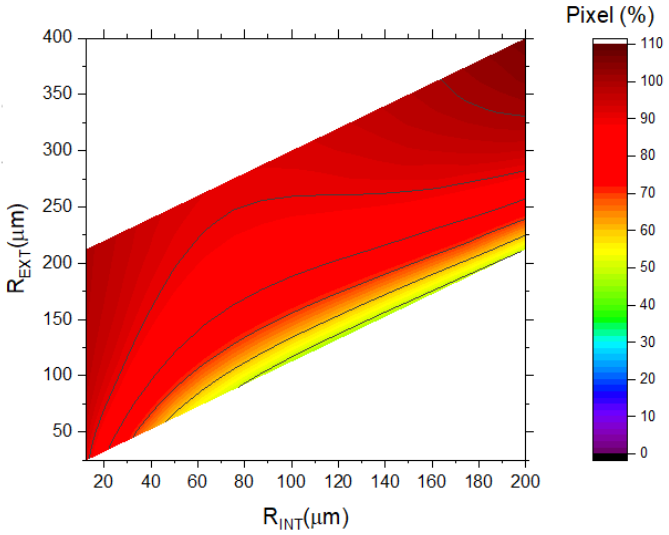

Figure. 7. % Pixel in respect to RINT and REXT for e = 100 µm and Hc = 35 µm.

Figure 7 presents a contour map of the % of the pixel for different combinations of R_{INT} and R_{EXT}, with a thickness e and a coil height H_C fixed. The values vary from 46.8% to 106.2%. The maximum values are achieved at R_{INT} = 200 µm and R_{EXT} = 400 µm. In this case, the magnetizing field in the proximity of the coils is even larger than in the axis because the pixel diameter, given by R_{INT}, is very large. The minimum values are achieved at R_{INT} = 100 µm and R_{EXT} = 135 µm. This case has a very sharp decrease from the axis to the beginning of the coil. There is a vast number of combinations where % Pixel remains between 85-95%.

Combining figure 6 and figure 7, we can determine that a combination around R_{INT} = 125 µm and R_{EXT} = 250 µm is a good trade-off between high magnetizing field, high % Pixel and pixel diameter without excessive coil thickness.

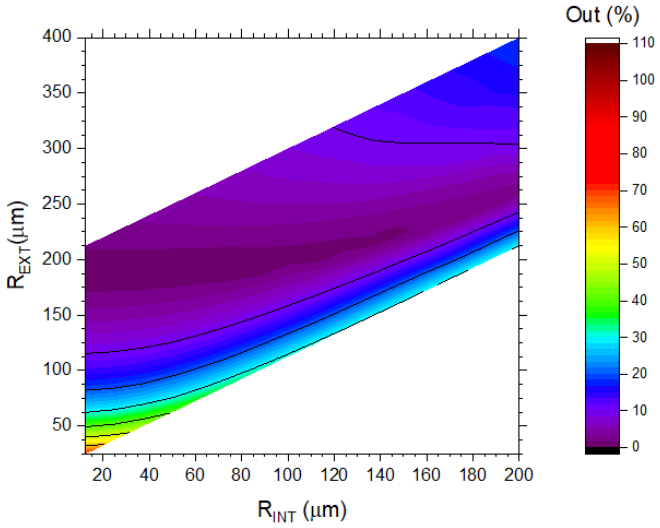

Figure 8. % Out in respect to RINT and REXT for e = 100 µm and Hc = 35 µm.

Figure 8 presents a contour map of the % Out for different combinations of R_{INT} and R_{EXT}, with a thickness e and a coil height H_C fixed. The values vary from 0% to 53%. The maximum values are achieved at R_{INT} = 125 µm and R_{EXT} = 25 µm. In this case, the magnetizing field outside the coil is very larger for an adequate pixel resolution, affecting significantly to adjacent volumes. The minimum values are achieved at R_{INT} = 15 µm and R_{EXT} = 200 µm. This case has a negligible effect on the adjacent volumes. Again, there is a vast number of combinations where % Out remains between 0-10%.

For the pre-selected combination of R_{INT} = 125 µm and R_{EXT} = 250 µm, the % Out is 5% which reinforces the trade-off benefits for this combination.

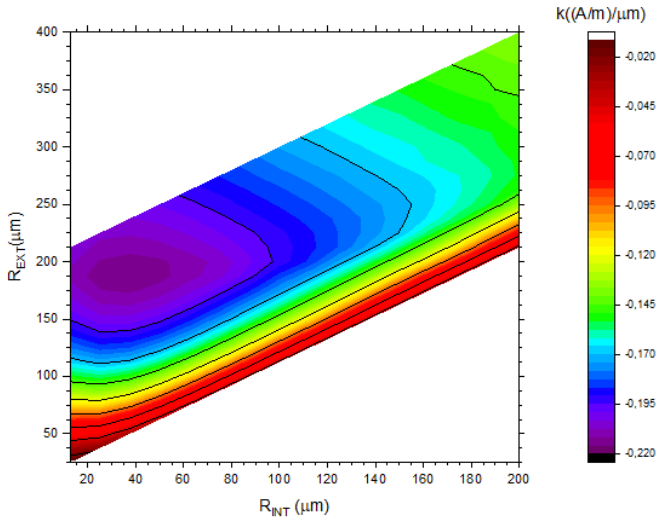

Figure 9. k in respect to RINT and REXT for e = 100 µm and Hc = 35 µm.

Figure 9 shows a contour map of the slope k for different combinations of R_{INT} and

R_{EXT}, with a thickness e and a coil height H_C fixed The values for k vary from -0.02 to -0.2 A/m/ µm for a current of 1 A/mm^2. The maximum values are achieved at R_{INT} = 25 µm and R_{EXT} = 200 µm. This means that the sharper decrease occurs for relatively thick coils. The minimum values are achieved at R_{INT} = 125 µm and R_{EXT} = 2.50 µm. In conclusion, the remanent magnetizing field out of the coil will still be significant, in agreement with conclusions from figure 8.

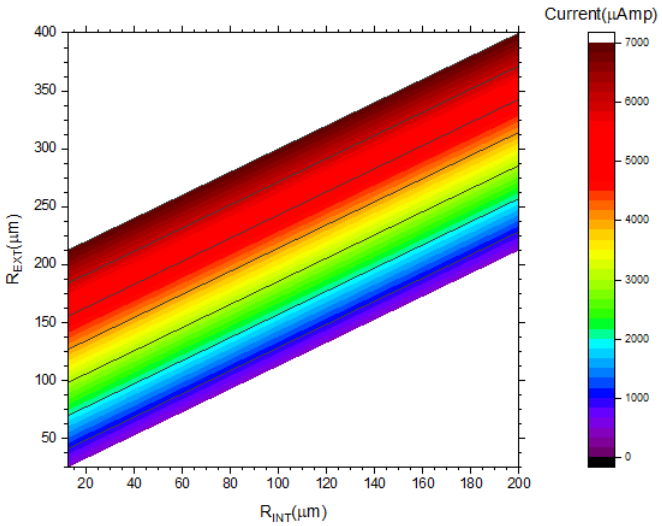

Figure 10. Currents in respect to RINT and REXT for e = 100 µm and Hc = 35 µm.

Total current flowing through a cross-section is proportional to (R_{EXT} – R_{INT}), i.e coil width. This behavior is described in figure 10. Minimum values for the total current are found in those combinations with thinner section while maximums are for the thicker ones. The order of magnitude in figure 10 is micro-ampere. This figure can be used to determine the total current for the magnetizer.

6. Application case

The level of current density necessary to magnetize a certain material is directly related to the material coercivity. The coercivity, also called the magnetic coercivity, coercive field or coercive force, is a measure of the ability of a ferromagnetic material to withstand an external magnetic field without becoming demagnetized. For ferromagnetic material the coercivity is the intensity of the applied magnetic field required to reduce the magnetization of that material to zero after the magnetization of the sample has been driven to saturation. General values of the coercivity for different materials are listed in table 2.

Material	Coercivity (kA/m)
Supermalloy	0.0002
Permalloy	0.0008-0.08
Iron filings	0.004-37.4
Electrical steel	0.032-0.072
Raw iron	0.16
Nickel	0.056-23.07
Cobalt	0.8-71.62
Ferrite magnet	125-250
Alnico magnet	40-150
Neodymium-iron magnet	800-1040
Samarium-cobalt magnet	600-800

Table 2. Coercivity of different materials.

Therefore, in order to fully magnetize a pixel, it is necessary to apply a current density high enough to generate a magnetic field in the H_{AXIS} point larger than the coercive for the corresponding material. Lower value of the magnetic field will partially magnetize the pixel. From this point, the shape of the resulting magnetization is given by the parameters % out and % pixel.

For example, let's magnetize a pixel of 100 μm of inner radius in NdFeB material. This means that the magnetic field intensity in the HAxis point has to be 800 kA/m. Arbitrarily we select 150 μm as outer radious of the coil, then, from figure 6 we obtain a magentic field value of 13 A/m. As the magnetic filed intensity is directly proportional to current density, the magnetizer should inject a current density of 61 kA/mm^2. In terms of total current means 123.67 A. If this total current is applied, the whole pixel axis will be magnetized since Haxis point has the lowest magnetic field in the axial length. In order to characterize the magnetization along the radius, % Out and % Pixel parameters must be analyzed. The RINT and REXT combinatio returns % Pixel = 70% and % Out = 10%. This means that the pixel in the RINT radial position will be magnetized only 70% of the total magnetization in the axis and that the magnetizing field outside the coil will still be a 10%. Therefore, for a proper magnetization of the whole pixel extra current should be applied, nevertheless, this extra current will affect adjacent pixels in a 10%.

7. Conclusions

The present work intends to calculate 2D multipole magnetization printing applied to the micro-magnets scale. The first step is the trade-off analysis to minimize the needed current for a certain magnetizing field level while keeping a good pixel size.

In this work, this first step is presented and applied to thin film micro-magnets of 100 µm thick. The dependence of the magnetizing field with respect to the geometrical parameter of the fixture is analyzed. An example of application of the results is given. Some design recommendations are:

- The thicker is the coil, the larger the magnetizing field. However, by using thicker coils the pixel will also be larger, decreasing the pattern resolution.
- There is a vast number of geometrical combinations where % Pixel remains between 85-95%.
- There is a vast number of combinations where % Out remains between 0-10%.
- An optimal selection for the coil height is a height similar to the coil thickness.
- The geometrical dependence is the same for the three orders of magnitude analyzed.
- Volumetric Joule effect heat is independent of the geometry of the coil.

Therefore, the results and conclusions presented in this work will permit to accelerate significantly trade-off procedures when designing 2D multipole magnetization patterning fixtures for specific industry applications.

Acknowledgments

This work has been funded by Universidad de Alcalá, under Grant No.CCGP2017-EXP/011.

References

[1] X. Ding, G. Liu, Z. Zuo, and H. Guo, “Improved differential-evolution based optimization design of an axial flux MEMS micromotor,” *Int. J. Appl. Electromagn. Mech.*, vol. 53, no. 4, pp. 645–661, Apr. 2017.

[2] M. Hahn, M. Bedenbecker, and H. H. Gatzen, “Evaluation of a Linear Hybrid Microstep Motor by Means of Magnetic Flux Measurements,” *IEEE Trans. Magn.*, vol. 43, no. 6, pp. 2588–2590, Jun. 2007.

[3] E. Diez-Jimenez, J.-L. Perez-Diaz, and J. C. Garcia-Prada, “Local model for magnet–superconductor mechanical interaction: Experimental verification,” *J. Appl. Phys.*, vol. 109, no. 6, pp. 063901-063901-5, 2011.

[4] E. Diez-Jimenez, “Design and analysis of a non-hysteretic passive magnetic linear bearing for cryogenic environments,” *Proc. Inst. Mech. Eng. Part J J. Eng. Tribol.*, 2014.

[5] R. Rizzo, A. Musolino, and H. C. Lai, “An Electrodynamic/Magnetorheological Clutch Powered by Permanent Magnets,” *IEEE Trans. Magn.*, vol. 53, no. 2, pp. 1–7, Feb. 2017.

[6] E. Diez-Jimenez, R. Sanchez-Montero, and M. Martinez-Muñoz, "Towards miniaturization of magnetic gears: Torque performance assessment," *Micromachines*, vol. 9, no. 1, p. 16, Dec. 2017.

[7] H. Lee, M. D. Noh, and Y.-W. Park, "Optimal Design of Electromagnetic Energy Harvester Using Analytic Equations," *IEEE Trans. Magn.*, vol. 53, no. 11, pp. 1–5, Nov. 2017.

[8] A. Laczko (Zaharia), S. Brisset, and M. Radulescu, "Design of a brushless DC permanent-magnet generator for use in micro-wind turbine applications," *Int. J. Appl. Electromagn. Mech.*, vol. 56, pp. 3–15, Feb. 2018.

[9] C. K. Lee and B. I. Kwon, "Study in the post-assembly magnetization method of permanent magnet motors," in *International Journal of Applied Electromagnetics and Mechanics*, 2004, vol. 20, no. 3–4, pp. 125–131.

[10] Min-Fu Hsieh, Yao-Min Lien, and D. G. Dorrell, "Post-Assembly Magnetization of Rare-Earth Fractional-Slot Surface Permanent-Magnet Machines Using a Two-Shot Method," *IEEE Trans. Ind. Appl.*, vol. 47, no. 6, pp. 2478–2486, Nov. 2011.

[11] E. Diez-Jimenez, A. Musolino, R. Rizzo, and E. Tripodi, "Analysis of the static and dynamic behavior of a non hysteretic superconductive passive magnetic linear bearing by using an electromagnetic integral formulation," *Prog. Electromagn. Res. M*, vol. 50, pp. 183–193, 2016.

[12] G. Bavendiek, K. Hameyer, M. Filippini, and P. Alotto, "Analysis of impulse-magnetization in rare-earth permanent magnets," *Int. J. Appl. Electromagn. Mech.*, vol. 57, pp. 23–31, Apr. 2018.

[13] Y. N. Zhilichev, "Precise multipole magnetization of disc magnet for sensor application," *IEEE Trans. Magn.*, vol. 39, no. 5, pp. 3301–3303, Sep. 2003.

[14] J. B. Bartolo, P. Klimczyk, K. Tiwisina, P. Denke, S. Siebert, and C. Gerada, "An investigation into the geometric parameters affecting field uniformity in four pole magnetisers," *Int. J. Appl. Electromagn. Mech.*, vol. 48, no. 2,3, pp. 225–232, Jun. 2015.

[15] J. Töpfer and V. Christopher, "Multi-pole magnetization of NdFeB sintered magnets and thick films for magnetic micro-actuators," *Sensors Actuators, A Phys.*, vol. 113, no. 2, pp. 257–263, 2004.

[16] A. Garraud, N. M. Dempsey, and D. P. Arnold, "Microscale magnetic patterning of hard magnetic films using microfabricated magnetizing masks," in *Proceedings of the IEEE International Conference on MEMS*, 2014, pp. 520–523.

[17] "Ansoft Ansys Maxwell v15 - Help assistant." 2018.

[18] W. H. Hayt, *Engineering Electromagnetics*. 1989.

View publication stats